

Surface Functionalizing Woody Biochar with UV Irradiation to Promote Adsorption of Heavy Metals

Yin Wang,^a Xiaolan Zeng,^b Qiao Li,^a Jiyuan Jin,^a Shuang Xiao,^b Xiaotang Xu,^a and Wenchuan Ding^{b,*}

To promote adsorption capacity of biochar as engineering material, pinewood biochar (PC) and bamboo biochar (BC) were prepared by slow pyrolysis (700 °C) and then directly irradiated with UV light at room temperature. The elemental analysis, SEM, FTIR, XPS, and Boehm titration measurements showed that UV irradiation significantly increased the BET surface area, porosity, and surface oxygen functional groups of the biochar. After UV treatment, the BET surface areas of PC and BC were increased by 63.0% and 217%, while the amount of total (acidic) groups increased by 62.0% (155%) and 24.9% (28.2%), respectively. FTIR and XPS measurements suggested that photochemical reactions, including photodegradation and photooxidation processes, may play primary roles in altering biochar the pore structure and surface functional groups of biochar. The Langmuir model capacities (q_{max}) of modified PC and BC were increased by 94.5% and 50.5% for Pb (II), 18.5% and 13.7% for Cd (II), respectively, compared to their unmodified counterparts. This study examined the effects of UV irradiation on the surface properties of biochar and demonstrate its potential as an effective, simple, and green method for functionalizing biomass material.

DOI: 10.15376/biores.19.4.7566-7590

Keywords: Adsorption; Biochar; Heavy metal; Photooxidation; Ultraviolet irradiation

Contact information: a: Power China Chengdu Engineering Corporation Limited, Chengdu, 610072, China; b: Three Gorges Reservoir Area's Ecology and Environment Key Laboratory of Ministry of Education, Chongqing University, Chongqing, 400045, China;

* Corresponding author: dingwenchuan@cqu.edu.cn

INTRODUCTION

Industrial activities related to mining operations, metal plating, petroleum refining, tanneries, batteries, pesticides, paints, and pigment manufacturing generate a large amount of waste streams containing high concentrations of heavy metals (Asuquo *et al.* 2017). Heavy metals (HMs) such as lead (Pb), cadmium (Cd), copper (Cu), mercury (Hg), and chromium (Cr) are highly toxic to many living organisms due to their acute and chronic lethal effects (Singh *et al.* 2021). Therefore, wastewater containing HMs must be treated to reduce the concentration to a prescribed level prior to being discharged into the environment. Technologies have been established to remove heavy metal ions from aqueous solutions, including chemical precipitation, ion exchange, flotation, electrochemical techniques, membrane separation and adsorption (Singh *et al.* 2021; Zeng *et al.* 2024). Among the mentioned treatments, adsorption is an attractive process with the advantages of wide adaptability, simple operation, and the possibility of metal recovery. Many inorganic minerals and organic carbon materials have been currently used as sorbents for HMs removal (Xiao *et al.* 2017). The sorbent has a crucial impact on the

economic and performance aspects of the adsorption process. Therefore, the development of high efficiency and low-cost materials is still needed. Biochar is a carbonaceous material that can be produced from biomass by a pyrolysis process. It has a unique structure and physicochemical properties that are receiving attention as an emerging sorbent for the removal of organic pollutants, nutrients, and HMs (Liu and Zhang 2009; Liu *et al.* 2019; Yin *et al.* 2018; Hou *et al.* 2022) in water. Biochar products are considered affordable and sustainable because they can be produced from a wide range of renewable sources in agriculture, forestry and municipal industries such as crop straw, livestock manure, branch and sawdust, and sewage sludge (Li *et al.* 2017). Unfortunately, biochar generally has a low specific surface area and fewer chemical groups, such that it exhibits a relatively low adsorption capacity. Therefore, exploring appropriate modification methods to enhance the adsorption performance of biochar is of great interest.

Over the past decade, physical and chemical modifications have been investigated to improve biochar adsorption performance on HMs. Physical methods are usually performed by heating or soaking with gaseous CO₂ or steam under relatively high temperatures, which significantly increases the surface area and pore volume of biochar (Zhang *et al.* 2014; Li *et al.* 2017). However, thermal treatment is energy-intensive and eliminates some of the surface functional groups because these moieties could be decomposed under high temperature conditions (Zhang *et al.* 2014). In contrast, chemical treatments have been extensively studied because, in many cases, they improve the porous structure as well as enrich the surface chemical groups (Chu *et al.* 2019; Kumar *et al.* 2022). The most commonly used chemical methods include acid and alkali treatment, surface oxidation, functional substance coating, and functional group anchoring (Hou *et al.* 2022; Kumar *et al.* 2022). However, conventional chemical treatments involve relatively complicated operations and result in secondary pollution.

Recently, UV irradiation has attracted great attention for its application in materials science. Previous studies have demonstrated that UV irradiation can alter the microstructural, chemical, and mechanical properties of organic material as an applicable method for material synthesis, performance evaluation and surface modification (Parekh *et al.* 2006; Cheng *et al.* 2012; Wang and Liu 2013; Raja 2015). These efforts reveal that UV irradiation has remarkable influences on the surface chemistry of carbonous materials. For example, under the exposure of UV irradiation, -CH₂ was gradually depleted, accompanied by the increase of carbonyl and hydroxyl groups on the surface of a styrene-butadiene-styrene copolymer (Tan *et al.* 2010). UV irradiation also gave rise to the formation of carboxylic functional groups on the surface of carbon nanotubes (Raja 2015). The results implied that UV light has potential applications to functionalize the biochar by changing the surface properties. In addition, UV modification has many advantages, such as a simple procedure, room temperature reactions, integrated operation settings, and no additional chemicals. The authors' previous research showed that UV irradiation substantially affected the surface properties of biochar and promoted the adsorption capacity for gaseous benzene and toluene (Li *et al.* 2016). Peng *et al.* (2018) reported an 18-fold increase in the sorption of aqueous Cr (VI) on the UV modified biochar compared to the pristine biochar. These investigations indicated that UV irradiation increased both the specific surface area and oxygen functional groups of biochar. However, the study of modification mechanisms on biochar surface under UV irradiation has been limited. Meanwhile, research on biochar from woody biomass is lacking, which is different in texture and physicochemical nature from the reported biochar from fruit shell (Li *et al.* 2016) and herbaceous biomass (Peng *et al.* 2018). The knowledge gained will be conducive

to further understanding and evaluating the potential of UV irradiation for functionalizing biochar.

In this study, bamboo biochar and pinewood biochar were employed to compare the outcomes of UV irradiation. The interfacial chemical behavior with respect to UV photochemical reactions on different biochar materials was then analyzed through surface physicochemical property measurements. Adsorption experiments were conducted to evaluate the effect of UV modification on HMs removal of biochar. The main objectives of this study are to explore the physical and chemical characteristics of biochar modified by UV light irradiation and the reaction mechanisms. Additionally, the influences of UV modification on the Pb (II) and Cd (II) ions adsorption performance of biochar are also considered.

EXPERIMENTAL

Biochar Preparation

Pinewood and bamboo strips were obtained as feedstock from a local timber processing plant in Chongqing, China. After being rinsed with pure water and oven dried (80 °C for 24 h), the feedstocks were fed into a tubular furnace (KFT, Qianjing Corp., China) where nitrogen gas was purged at the flux of 300 mL min⁻¹ to expel oxygen during carbonization. The biomass was carbonized at pyrolytic temperature of 700 ± 1 °C for 1.0 h. Then the solid residues (*i.e.*, biochar) were crushed for sieving to 0.20 to 0.35 mm particle size. The granular biochar samples were mixed with a 10% (v/v) hydrochloric acid solution for 12.0 h and rinsed three times with pure water to remove impurities. Finally, the products were oven dried at 105 ± 1 °C for 24 h and stored in a desiccator as original biochar for future use.

UV Modification

UV modification was performed in a chamber with a 1000 W high-pressure mercury lamp (XZC1000, Xingzhucheng Corp. China). The wavelengths of the lamp ranged from 350 to 450 nm with a major peak at 365 nm. A pre-weighed 10.0 g amount of original biochar was layered in a flat bottom ceramic disc (diameter = 7.0 cm), and then the disc was placed under the UV lamp at a distance of 8.0 cm. The biochar samples were irradiated for 16.0 h according to the result of an iodine value assessment carried out previously (Fig. S1). The samples were then re-sieved to a particle size of 0.20 to 0.35 mm and were ready for testing without further treatment. The biochar samples were referred to pinewood char (PC), bamboo char (BC), modified pinewood char (MPC) and modified bamboo char (MBC), respectively.

Biochar Characterization

The pH of the biochar was measured using a model PHS-3E pH meter (Shanghai INESA Corp., China). The pH was evaluated for the solution in which the biochar was mixed with 1:20 solid to water ratio for 0.5 h of shaking. Elemental analysis of the biochar bulk was performed using a CHONS elemental analyzer (Vario EL III, Elementar Company, Germany), calculating O content by weight difference between the sample and the sum of C, H, and N. The elemental composition of the biochar surface was determined by X-ray photoelectron spectroscopy (XPS, ESCALAB250Xi, Thermo Fisher, USA). The survey scans and high-resolution scans for C 1s and O 1s were achieved by monochromatic

Al K α radiation. The binding energy of the spectra was calibrated by setting the C 1s sp² hybridized electrons to 284.8 eV. The spectra were fitted using the Avantage software package V5.976 (Thermo Fisher Scientific Corp., USA). Cation exchange capacity (CEC) was determined following the ammonium acetate (NH₄OAc) method, as described in reference (Carter and Gregorich 2006). The Brunauer-Emmett-Teller (BET) surface area, pore volume, and pore size distribution were determined using a Micromeritics ASAP 2020 nitrogen adsorption apparatus (Micromeritics, Co., USA) at 77 K. Fourier transform infrared spectroscopy (FTIR) analysis was performed using a Nicolet 5DXC FTIR spectrometer (Thermo Scientific Company, USA) to characterize the surface functional groups. The infrared spectra were collected in a range of 400 to 4000 cm⁻¹ with a resolution of 4.0 cm⁻¹. The Boehm titration method was used to quantitatively determine the oxygen containing functional groups on the biochar surface based on the reference (Karthik *et al.* 2023). The physical morphology of biochar surface was examined using a scanning electron microscope (Nava 400 FEG-SEM, USA) under an acceleration voltage of 10.0 kV.

Adsorption Experiments

All chemicals were analytical grade. Stocking solutions of Pb (II) and Cd (II) ions were prepared by dissolving Pb (NO₃)₂ and Cd (NO₃)₂ in deionized water at metal concentrations of 1000 mg L⁻¹. In batch sorption experiments, 0.15 g of sorbent was added to a 50 mL stoppered polypropylene vessel containing 25.0 mL of Pb (II) or Cd (II) solution. The initial solution pH was adjusted with 0.1 M HNO₃ or NaOH solutions. The vessel was agitated on a shaker at 150 rpm under 25±1.0 °C. For the adsorption kinetic study, the initial pH was adjusted to 5.0 and the concentrations of Pb (II) and Cd (II) solution were of 200.0 mg L⁻¹ and 100.0 mg L⁻¹, respectively. The suspension in the vessel was extracted and filtered through a 0.45 μm nylon membrane at predetermined time intervals. The concentration of the remaining metal ions in solution was determined using a TAS-990 atomic absorption spectrophotometer (Persee Corp., China). Adsorption isotherms were carried out at initial pH of 5.0 and initial concentrations of Pb (II) and Cd (II) ranging from 30.0 to 800.0 mg L⁻¹ and from 10.0 to 500.0 mg L⁻¹, respectively. The mixture was agitated at 150 rpm, and the equilibrium was reached in 24.0 h. The effect of initial pH value (2.0 to 6.0) on the sorption capacity was also investigated.

Data Analysis

The adsorption capacity of biochar for HMs ions removal was calculated as follows,

$$q_e = \frac{(C_0 - C_e)V}{W} \quad (1)$$

where q_e is the HMs amount per unit weight of biochar sorbing at equilibrium (mg g⁻¹); C_0 and C_e are the initial and equilibrium sorbate concentration in solution (mg L⁻¹); W is the mass weight of biochar (g), and V is the solution volume (L).

The sorption kinetics was simulated using three mathematical models, *i.e.*, pseudo-first-order, pseudo-second-order, and simple Elovich models (Jin *et al.* 2014), as follows,

$$\text{First-order: } \ln(q_e - q_t) = \ln q_e - k_1 t \quad (2)$$

$$\text{Second-order: } \frac{t}{q_t} = \frac{1}{k_2 q_e^2} + \frac{1}{q_e} t \quad (3)$$

$$\text{Elovich: } q_t = \alpha + \beta \ln t \quad (4)$$

where q_t is the mass of metals adsorbed onto biochar at time t (mg g^{-1}), k_1 (h^{-1}) and k_2 ($\text{g mg}^{-1}\text{h}^{-1}$) are the first-order and second-order sorption rate constants, α ($\text{mg g}^{-1}\text{h}^{-1}$) is the initial adsorption rate and β (mg g^{-1}) is the Elovich constant.

The Langmuir, Freundlich, and Temkin models were used to fit the experimental data of the sorption isotherms (Manfrin *et al.* 2021),

$$\text{Langmuir model: } q_e = \frac{q_m K_L C_e}{1 + K_L C_e} \quad (5)$$

$$\text{Freundlich model: } q_e = K_F C_e^{\frac{1}{n}} \quad (6)$$

$$\text{Temkin model: } q_e = b \ln(K_T C_e) \quad (7)$$

where q_m is the Langmuir maximum sorption capacity (mg g^{-1}), K_L is the Langmuir constant related to sorption energy (L mg^{-1}), K_F is the Freundlich affinity coefficient ($\text{mg}^{(1-n)} \text{L}^n \text{g}^{-1}$), n is the Freundlich linearity constant, b is the Temkin isotherm constant, and K_T is the isotherm equilibrium binding constant (L g^{-1}). The essential features of the Langmuir isotherm was expressed in terms of separation parameter R_L , which could be used to evaluate whether an adsorption system is favorable or unfavorable (Zhao *et al.* 2021). The R_L value indicates that the sorption is either irreversible ($R_L=0$), favorable ($0 < R_L < 1$), linear ($R_L=1$), or unfavorable ($R_L > 1$).

$$R_L = \frac{1}{1 + K_L C_e} \quad (8)$$

All sorption experiments were carried out in duplicate, and the mean values were reported. The model of the best fit was determined by the coefficient of determination (R^2) which was calculated according to linear regression analysis of the models. The normalized standard deviation (NSD) was calculated in to compare the prediction accuracy of different kinetic models (Wang *et al.* 2015),

$$\text{NSD} = 100 \times \sqrt{\frac{\sum [(q_{t,\text{exp}} - q_{t,\text{pred}})/q_{t,\text{exp}}]^2}{n-1}} \quad (9)$$

where $q_{t,\text{exp}}$ and $q_{t,\text{pred}}$ are the experimental value and the calculated value of models corresponding to reaction time, respectively, and n is the number of data point.

RESULTS AND DISCUSSION

Characterization of UV Irradiated Biochar

Elemental composition

UV irradiation substantially increased oxygen contents of the biochar, which was confirmed by elemental analysis (Table 1). Original biochar BC and PC were carbon-rich with carbon contents over 88%, but less oxygen, hydrogen, and nitrogen, indicating that the feedstock biomass had become highly carbonized at the 700 °C pyrolytic temperature. The carbon contents were found to decrease significantly after UV treatment. In contrast, the oxygen contents increased dramatically from 8.21% (BC) to 12.85% (MBC), and from 8.51% (PC) to 19.15% (MPC), respectively. The variation of carbon and oxygen contents in biochar suggested the occurrence of oxidation on biochar during UV irradiation. It was noteworthy that the molar O/C ratios of MBC and MPC increased by 65% and 160%, respectively, compared to PC and BC, indicating more hydrophilic and higher polar groups

on modified biochar (Karthik *et al.* 2023). The hydrogen and nitrogen contents of modified biochar were slightly lower than those of the pristine. No significant differences in the molar H/C ratio were found between the original and modified chars. The low H/C ratios (0.003 to 0.013) indicated that all samples retained high aromatic structures (Chen *et al.* 2008).

Table 1. Summary of Characteristics of the Materials

Properties	BC	MBC	PC	MPC
C (%)	88.76	84.29	88.95	76.78
N (%)	1.30	1.18	1.46	1.35
O (%)	8.21	12.85	8.51	19.15
H (%)	1.17	1.06	0.31	0.20
ratio O/C	0.093	0.152	0.096	0.249
ratio H/C	0.0132	0.0126	0.0035	0.0026
S_{BET} ($\text{m}^2 \cdot \text{g}^{-1}$)	141.73	449.13	280.86	457.72
$^a S_{\text{micro}}$ ($\text{m}^2 \cdot \text{g}^{-1}$)	119.34	341.44	241.40	356.41
$^b S_{\text{exter}}$ ($\text{m}^2 \cdot \text{g}^{-1}$)	22.39	107.69	39.46	101.31
$^c V_{\text{total}}$ ($\text{m}^3 \cdot \text{g}^{-1}$)	0.07	0.25	0.14	0.27
$^d V_{\text{micro}}$ ($\text{m}^3 \cdot \text{g}^{-1}$)	0.06	0.16	0.11	0.16
$^e D_{\text{aver}}$ (nm)	2.07	2.21	1.95	2.32
pH	6.21	5.90	7.60	6.56
CEC ($\text{cmol} \cdot \text{kg}^{-1}$)	1.73	4.35	1.47	4.00
Carboxylic ($\text{mmol} \cdot \text{g}^{-1}$)	0.561	0.584	0.211	0.351
Phenolic ($\text{mmol} \cdot \text{g}^{-1}$)	0.073	0.080	0.040	0.071
Lactonic ($\text{mmol} \cdot \text{g}^{-1}$)	0.204	0.410	0.119	0.522
Acidic ($\text{mmol} \cdot \text{g}^{-1}$)	0.838	1.074	0.370	0.944
Basic ($\text{mmol} \cdot \text{g}^{-1}$)	0.197	0.219	0.527	0.509
Total ($\text{mmol} \cdot \text{g}^{-1}$)	1.035	1.293	0.897	1.453
$^a S_{\text{micro}}$: Micropore area determined by t-plot method.				
$^b S_{\text{exter}}$: External surface area determined by t-plot method.				
$^c V_{\text{total}}$: Total pore volume determined at $P/P_0 = 0.99$.				
$^d V_{\text{micro}}$: Micropore volume determined by t-plot method.				
$^e D_{\text{aver}}$: Average pore diameter obtained from BJH equation using N_2 isotherms at -196°C .				

Surface functional groups

The distribution of functional groups on the biochar surface was revealed by FTIR measurement, as shown in Fig. 1. The infrared spectra of MBC (BC) were very similar, with four principal bands at wavenumbers of 3445 (3455 cm^{-1}), 1631 (1631 cm^{-1}), 1117 (1120 cm^{-1}), and 621 (625 cm^{-1}). The broad band near 3450 cm^{-1} was ascribed to $-\text{OH}$ stretching vibrations in phenolic hydroxyl groups (Zhao *et al.* 2021). The peak located at 1631 cm^{-1} was assigned to $\text{C}=\text{O}$ stretching vibration of carboxyl/carbonyl groups (Peng *et al.* 2018). The peak at about 1120 cm^{-1} was attributed to the aliphatic ether asymmetric $\text{C}-\text{O}-\text{C}$ stretching or the alcoholic $\text{C}-\text{O}$ stretching absorptions. The band at about 625 cm^{-1} was attributed to the $\text{N}-\text{H}$ out-of-plane bend. The FTIR spectra of pinewood biochar presented more absorption bands and peaks than those of bamboo biochar (Fig. 1). The presence of abundant surface functional groups can be attributed to the different chemical constitutions of the feedstocks. In addition to the hydroxyl group band at near 3450 cm^{-1} , the bands at 2924 cm^{-1} (PC) and 2923 cm^{-1} (MPC) were attributed to the asymmetric vibration of $-\text{CH}_2$ associated with methyl and methylene groups (Raja 2015). The other

peaks that appeared in all pinewood biochar spectra were associated with C – H bending vibration (1384 and 1385 cm^{-1}) of aldehydes, C – O – C stretching vibration (1102 and 1094 cm^{-1}) of ethers, and C – H out-of-plane bending (870 and 872 cm^{-1}) of aromatics (Jin *et al.* 2014), respectively. A remarkable peak at 1543 cm^{-1} appeared only in MPC with the co-occurrence of the peak at 1385 cm^{-1} , indicating that carboxylate anion groups $-\text{C}(=\text{O})_2^-$ were formed under UV irradiation. Moreover, the intensities of bands at 2924 cm^{-1} , 1385 cm^{-1} and 870 cm^{-1} in biochar PC decreased dramatically after UV treatment. This implied the elimination of some C – H groups on account of photochemical reaction on the biochar surface.

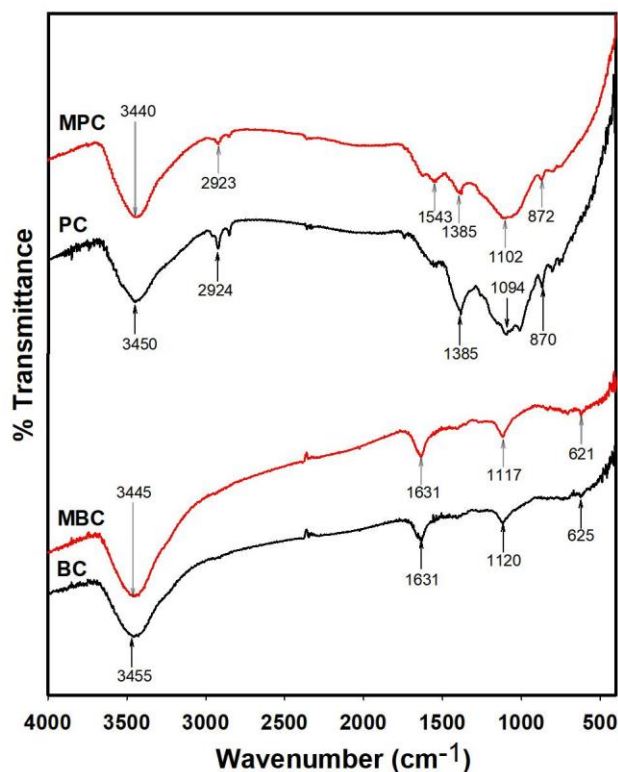


Fig. 1. FTIR spectra of biochars before and after UV irradiation

The Boehm titration data (Table 1) provided the quantitative analysis of surface functional groups, which resulted in the apparent surface acidity and basicity of the biochar (Karthik *et al.* 2023). The acidic groups on the UV irradiated biochar increased, while the basic groups had no significant change compared with those on the original biochar. For example, the amount of acidic groups increased by 28.2% for BC and 155.2% for PC, respectively. As expected, the pH values of the modified biochar were lower than their pristine forms. The acidic groups were oxygen containing functional groups such as carboxyl, carbonyl, quinone, hydroxyl, carboxylic anhydride, and lactone. Therefore, UV irradiation generated more oxygen-containing groups on the pinewood biochar than on the bamboo biochar, which was responsible for a greater pH decrease of MPC than MBC. The CEC values of modified biochar increased remarkably, which was ascribed to the increasing content of carboxylic groups (Trakal *et al.* 2014). It could be concluded that UV irradiation significantly increased the amount of oxygen containing functional groups, which had a great impact on the surface chemistry of biochar.

Surface area and pore distribution

As shown in Table 1, the BET surface area and pore volume of biochar were increased after UV modification. The S_{BET} of MBC and MPC were 217% and 63% higher than those of BC and PC, respectively. Meanwhile, both total pore volume and micropore volume increased. The increase in surface area and pore volume was mainly attributed to the development of pore structure as a result of UV irradiation. The average pore diameter of BC (2.07 nm) and PC (1.95 nm) mainly reflected the micropore and mesopore characteristics of the original biochar. After modification, about 10% increase in the average pore diameter of MBC (2.21 nm) and MPC (2.32 nm) was observed. The results indicated the transition from average micropore to mesopore on the surface of modified biochar. The differences between modified and pristine biochar were revealed by the nitrogen sorption isotherms shown in Fig. S2(a). The pristine biochar exhibited the Type I isotherm of the BDDT classification system (Brunauer *et al.* 1940). The Type I isotherm suggested the character of a microporous material where micropores were filled rapidly in a relatively low partial pressure (P/P_0) region. The modified biochar, however, exhibited Type IV isotherms. This isotherm type indicated a dominant mesopore structure on solid surface. The cumulative volume versus pore width (Å) curve (Fig. S2(b)) showed that the pore volumes of micropore and mesopore in modified biochar increased distinctly. However, the micro- and mesopore occupied a large proportion of the total pore volume both of pristine and modified biochar. Therefore, the increase in surface area after UV modification was due to the formation of both micropores and mesopores that augment the porosity of biochar.

Surface morphology

The visual physical changes of the biochar surface caused by UV irradiation were described by scanning electron microscopy (SEM) measurement (Fig. 2). The SEM images (5000×) of MBC and MPC showed that the modified biochar had a more intense porous structure on the surface than that of the unmodified biochar. The etching pits (marked yellow circle) were also found on the surface of MBC (Fig. 2d). Generally, the SEM measurements supported our conclusion that UV modification could promote the porosity of biochar and thus increased the surface area of biochar. The results were consistent with the findings reported in other publications (Li *et al.* 2016; Peng *et al.* 2018).

Surface oxidation on biochar

XPS analysis was conducted to further investigate the surface chemical changes of pinewood biochar under UV irradiation. The full XPS survey showed that both PC and MPC were composed of C 1s, O 1s, N 1s, and Si 2p (Fig. S3). The relative atomic percentage of each constituent element was quantitatively calculated from the deconvolution peak area of the fitted curve. The PC exposed to UV irradiation showed an increasing amount of oxygen from 8.9 at% to 17.9 at%, while the amount of carbon decreased from 87.4 at% to 77.4 at%. The O/C ratio (0.31) in the MPC surface almost tripled as the ratio (0.11) in the MPC bulk shown in Table 1. It suggested that the oxidation during UV irradiation occurred mainly on the biochar surface. The spectra of C 1s and O 1s regions for the PC and MPC are shown in Fig. 3. The possible species and their percentages are identified in Table 2 (Beamson and Briggs 1992; Kwan *et al.* 2015). As can be seen from the C 1s spectra (Fig. 3), both PC and MPC had peaks at the binding energy of ~284.7 eV, ~286.1 eV and ~288.4 eV which were assigned to C – C (graphitic),

C – O (hydroxyl)/C – O – C (ethers, epoxy) and O – C = O (ester, carboxyl), respectively. After UV irradiation, the content of C – C in PC surface had a remarkable decrease from 76.8% to 54.0%; meanwhile the content of C – O/C – O – C and O – C = O increased from 6.02% and 1.91% to 10.17% and 3.50%, respectively. The results indicated that the oxidation reaction primarily occurred at the carbon-carbon bonds to form carbon-oxygen bonds. The XPS measurement was consistent with the FTIR measurement (Fig.1). Compared with the PC (Fig.3a), the MPC (Fig.3b) had two additional peaks at the binding energy of 288.0 and 289.9 eV, which were assigned to C – O – C (ethers)/C = O (ketones) and O = C – O – C = O (anhydride)/O – (C = O) – O (carbonate). It suggested the further degradation or transformation of chemical groups during UV irradiation. The XPS O 1s spectra of PC and MPC showed the increasing content of oxygenic functional groups on biochar after UV irradiation, which was in accord with the results of C 1s spectra.

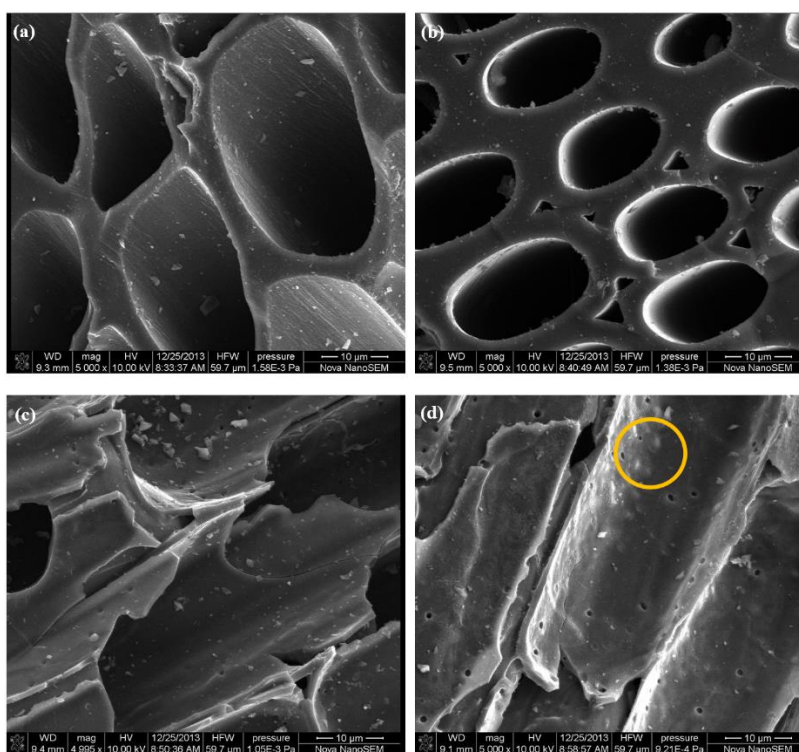


Fig. 2. SEM images of biochar (5000 \times): (a) PC, (b) MPC, (c) BC, (d) MBC

The conspicuous effects of UV irradiation on the surface of carbonaceous materials, *i.e.*, the formation of the oxygen-containing groups, have been observed by other researchers (Osbeck *et al.* 2011; Raja 2015; Peng *et al.* 2018). A previous study indicated that the elemental composition and the surface functional groups of biochar were little changed by UV irradiation under air isolation circumstance (Li *et al.* 2016). This suggested that oxygen played a main role in UV modification. In addition, the temperature of the biochar surface was increased to around 100 °C under the UV irradiation. In order to identify the effect of high temperature on surface properties variation, the original biochar was heated in the oven under 100 °C lasting the same as the UV irradiation and the iodine value assessment was carried out. The iodine value exhibited almost constant value versus the heating time (Fig. S1). Thus, high temperature by itself did not play a main role in

changing the surface properties of biochar. It could be speculated that oxygen atom [O] and ozone (O₃), derived from the photochemical reaction of oxygen molecule with UV irradiation, adhered to the surface of biochar, and lead to break the C – C bonds in the ring structure or oxidize the aliphatic sites to form carbon-oxygen bonds (Osbeck *et al.* 2011). One of the mechanisms could be elucidated as ozone addition to unsaturated sp² carbon bonds to form a primary ozonide, which followed bond cleavage to produce carbonyl compounds and a Criegee intermediate (Parekh *et al.* 2006). The products were subsequently decomposed, resulting in the formation of ester groups (O – C = O) and the release of gaseous CO₂ (Krysak *et al.* 2007). These reactions could be confirmed in the present study by the XPS analysis results that the contents of the O – C = O (ester, carboxyl) and C = O (ketones) in biochar increased after UV modification as shown in Table 2. Furthermore, anhydride/carbonate groups on MPC (289.9 eV) were detected. These moieties were the most oxidized form of bound carbon before the formation of carbon dioxide (Parekh *et al.* 2006).

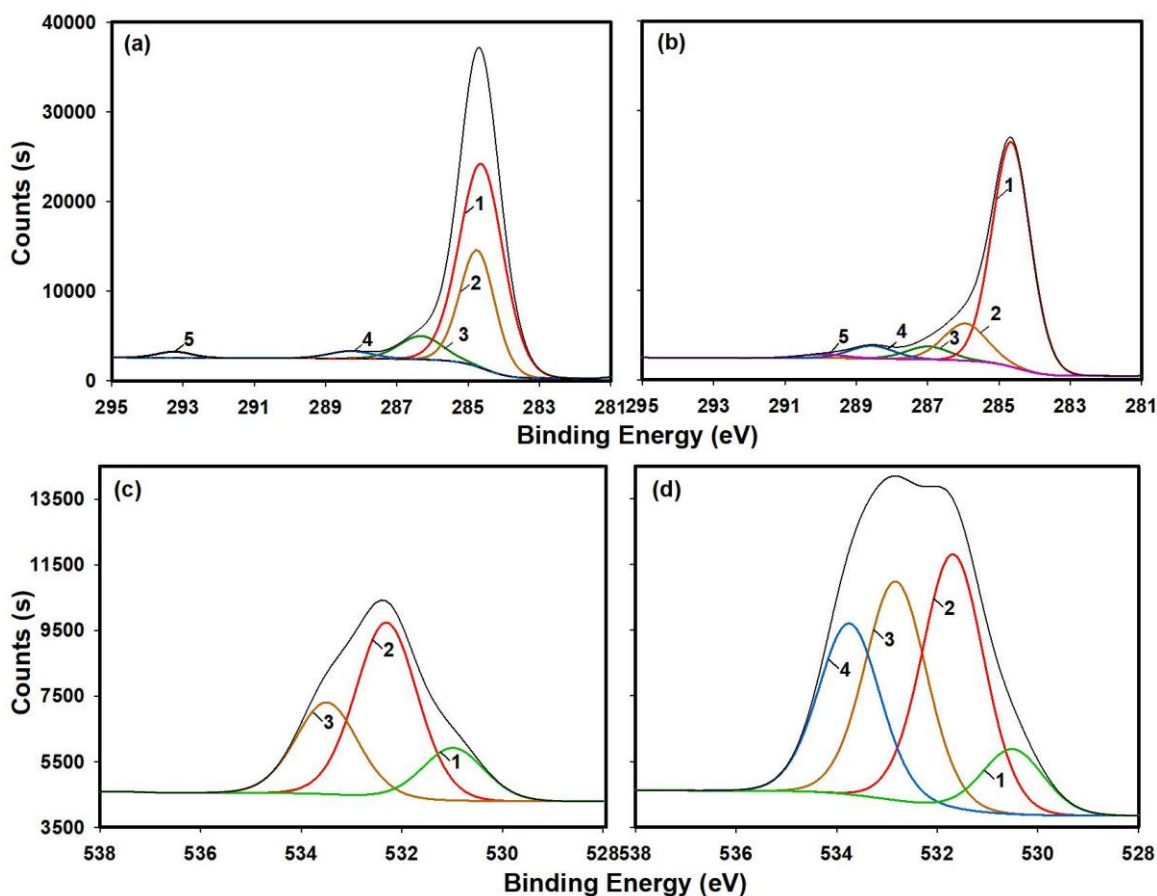
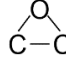


Fig. 3. C 1s and O 1s XPS spectra of the biochar: (a) C 1s of PC, (b) C 1s of MPC, (c) O 1s of PC, (d) O 1s of MPC

Table 2. Assignment of C 1s and O 1s Peaks by Binding Energy for BC and MBC

Element	Binding energy (eV), Peak		Functional groups	Atomic (%)	
	PC	MPC		PC	MPC
C 1s	284.64, 1	284.65, 1	C–C	76.80	54.02
	284.75, 2				
	286.33, 3	285.94, 2	C–OH, C–O–C, 	6.02	10.17
	ND	286.98, 3	C–O–C, C=O	--	3.53
	288.30, 4	288.57, 4	O–C=O,	1.91	3.50
	ND	289.93, 5	O=C–O–C=O, O–(C=O)–O	--	1.04
	293.24, 5	ND	Energy loss	1.26	--
O 1s	530.98	530.50	C=O	1.40	1.84
	ND	531.68	O–C–O, –C(=O)–O	--	7.19
	532.30	532.82	C=O, C–O–C	4.66	6.19
	533.49	533.75	O=C–O–C=O, O–C=O	2.45	4.84

UV irradiation had significant effects on the surface texture of biochar (Fig. 2). However, the mechanism of pore structure development on biochar surface under UV irradiation has not been extensively discussed. Based on the surface properties measurements and the previous studies, it is proposed that the formation of pores on treated biochar could be attributed to the result of photo oxidation induced by UV irradiation. These photochemical reactions involved photo degradation process and photo oxidation process. The wavelength of UV light adopted in this study was dominant in 365 nm, the energy generated by photon of this range was 328 kJ mol⁻¹. The C – C bond strength of polymer molecules is in the range 300 to 720 kJ mol⁻¹ (Asmatulu *et al.* 2011). Thus, the UV light could initiate direct photo dissociation on the biochar surface because the UV was energetic enough to break the partial C – C and unsaturated aromatic bonds (Ghasemi-Kahrizsangi *et al.* 2015). The secondary gasification reaction occurred directly towards the edges and the defects, in the presence of oxygen, to form oxidation products such as CO and CO₂. Then, the vacancies (holes) on the biochar surface were generated from the defect area. As the UV irradiation continued, the holes grew and the volatiles, CO₂ and CO molecules were released from the biochar, resulting in the formation of additional pores (Cheng *et al.* 2012). The photooxidation process was conducted by active oxygen species such as [O] and O₃ produced by UV irradiation (Kryszak *et al.* 2007; Raja 2015). Initially, the active oxygen species added across unsaturated bonds to form epoxy groups that weakened the previous C – C bond, resulting in the scission of the C – C bond (Li *et al.* 2006). The further attack by active oxygen atoms at defective sites induced the formation and subsequent release of CO and CO₂ molecules, which generated the oxidized monovacancies (Cheng *et al.* 2012). The consecutive oxidation process could enlarge the vacancies to form bigger holes. This would explain the formation of extra pores observed on the surface of modified biochar (Fig. 2b and 2d). However, the increase in pore size was restricted because the active oxygen species were eliminated through reverse reaction. For

example, the O_3 reacted with $[O]$ to form O_2 as $O_3 + [O] = 2O_2$, and O_3 was also decomposed to O_2 under the catalysis of carbon as $2O_3 + C = 3O_2 + C$. The concentration of active oxygen species decreased and the intensive oxidation reactions could not be sustained. Meanwhile, the formation of $C-O-C$ bonds replacing $C-C$ bonds increased the resistance to photo oxidation (Parekh *et al.* 2006). The primary photochemical reactions on the biochar surface under UV irradiation are shown in Fig. 4. However, the photooxidation involved not only the dissociation of carbon bond, but also the degradation or transformation of chemical groups on biochar. Moreover, the UV light is commonly subdivided into three regions: UVA (315-400 nm), UVB (280-315 nm) and UVC (100-280 nm). The photochemical effects of different wavelengths on biochar are unclear. Thus, further investigation of this topic is of interest.

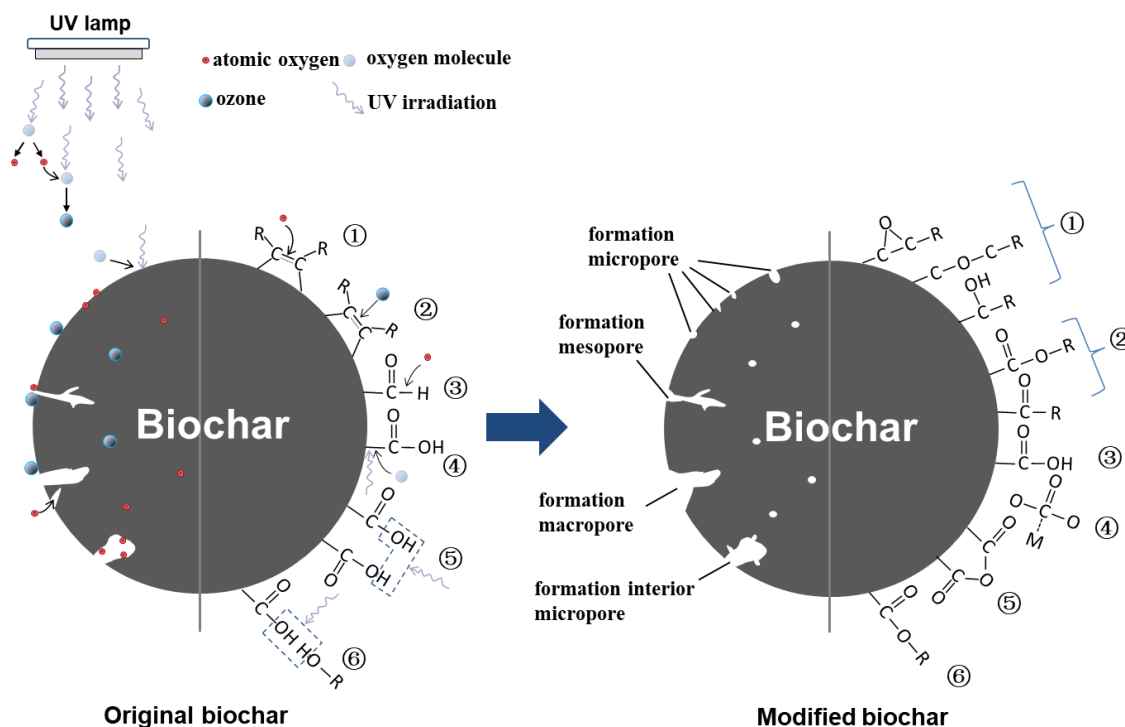


Fig. 4. Illustration of the photooxidation mechanism of UV irradiation on biochar surface -- pore development and oxygenic groups generation

Adsorption Studies

Adsorption kinetics

The effect of reaction time on metal ions adsorption by biochar is shown in Fig. 5. Typically, all biochar samples presented rapid initial sorption corresponding to 60% to 90% of the final adsorption within the first 3.0 h of reaction., and then the sorption increased slightly to approach equilibrium after 24.0 h. No further significant sorption occurred between 24.0 and 48.0 h. Compared with PC and BC, the metal ions sorbed by MPC and MBC at equilibrium increased by 134% and 73% for Pb (II) ions, 14.1% and 25.5% for Cd (II) ions, respectively. The increase in sorption was attributed to the ascending surface area and chemical groups, which created more binding sites on the modified biochar. The experimental data were fitted to three kinetic models, namely pseudo-first order, pseudo-second order, and Elovich equations to analyze the adsorption processes. The kinetic parameters of each model obtained from the regression results are

summarized in the supplementary materials (Table S1). Consistent with the previous research (Mohan *et al.* 2014), the determination coefficient (R^2) value of the second-order model was higher than other models for all tests. Meanwhile, the second-order model had the smallest NSD values among three models from data fitting in Pb(II) adsorption experiments. Therefore, the sorption of Pb (II) on all biochar samples was better described by a second-order model, suggesting a diffusion-limited mechanism determining the reaction rate (Hubbe *et al.* 2019). However, in Cd (II) adsorption, the Elovich model had smaller NSD values than other models, so the Elovich model was considered the best fit for Cd (II) adsorption. The Elovich model has also been widely used to describe chemical adsorption occurring on the sorbent surface (Wu *et al.* 2009). The result of the model fitting implied the discrepancy in the interfacial behaviors between Pb and Cd, which may be related to their hydrated radius, species in solution, and electron affinity. For instance, the hydrated radii of Pb (4.01 Å) were smaller than that of Cd (4.26 Å) (Nightingale 1959), it allowed Pb ions to enter smaller pores or penetrate through the porous surface to interact with the binding sites on the subsurface, therefore it had effects on the rate of binding process and adsorption capacity.

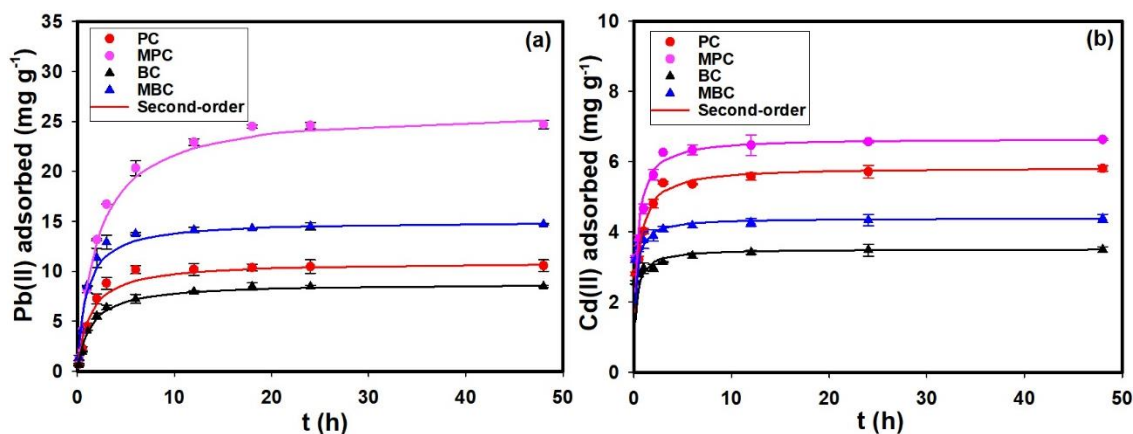


Fig. 5. Sorption kinetics of pristine and modified biochar: (a) Pb (II), (b) Cd (II)

Adsorption isotherms

The adsorption isotherms of Pb (II) and Cd (II) are plotted in Fig. 6. The shapes of the data curves of the biochar were similar to those observed in previous studies (Mohan *et al.* 2014). The amounts of metal ions sorbed on the modified biochar were obviously higher than the pristine at all concentrations. An interesting finding was that at an initial Pb(II) concentration below 200 mg g⁻¹, the ratios of adsorption capacity (q_e) of modified biochar vs. pristine biochar increased with increasing initial concentration. The maximum ratio value was reached at the initial concentration of 200 mg g⁻¹, after which the ratio values decreased slightly. For example, when the initial Pb(II) concentrations were 30, 200, and 600 mg g⁻¹, the q_e (MPC)/ q_e (PC) ratio and q_e (MBC)/ q_e (BC) ratio were 1.22, 2.34, 2.05, and 1.25, 1.72, 1.59, respectively. The data indicated that modified biochar was competitive in removing Pb(II) at relatively high concentration. The Cd(II) sorption was different from that of Pb(II), with the ratio values being almost constant over the concentration range. Adsorption isotherm models revealed the adsorption mechanism and expressed the surface properties of sorbents.

In this study, the experimental data were fitted by Langmuir model, Freundlich model, and Temkin model. The calculated parameters as well as the regression coefficients

are shown in Table 3. Three models described the experimental data well, but the Langmuir isotherm model fitted better than others due to the highest R^2 value. Meanwhile, the values of the separation parameter R_L for the experimental data were between 0 and 1 (Fig. S4), indicating the favorable adsorption system of heavy metals on biochar (Zhao *et al.* 2021). The maximum adsorption capacities obtained from Langmuir isotherm equations showed that Pb(II) binding on MPC and MBC were increased by 94.5% and 50.5%, while Cd (II) sorption of MPC and MBC were increased by 18.5% and 13.7%, comparing with their original. The pinewood char showed a stronger affinity to HMs than the bamboo char after modification. This was probably due to more functional groups and active surface area on pinewood char than on bamboo char after UV irradiation (Table 1). The proper irradiation parameters should be considered when UV irradiation is applied to functionalize biochar from various raw materials. A comparison of Pb and Cd adsorption capacities of sorbents reported in other literature (Table S2 and S3), indicating that MPC and MBC had comparable adsorption performances to many other biochar produced from ligneous plant biomass.

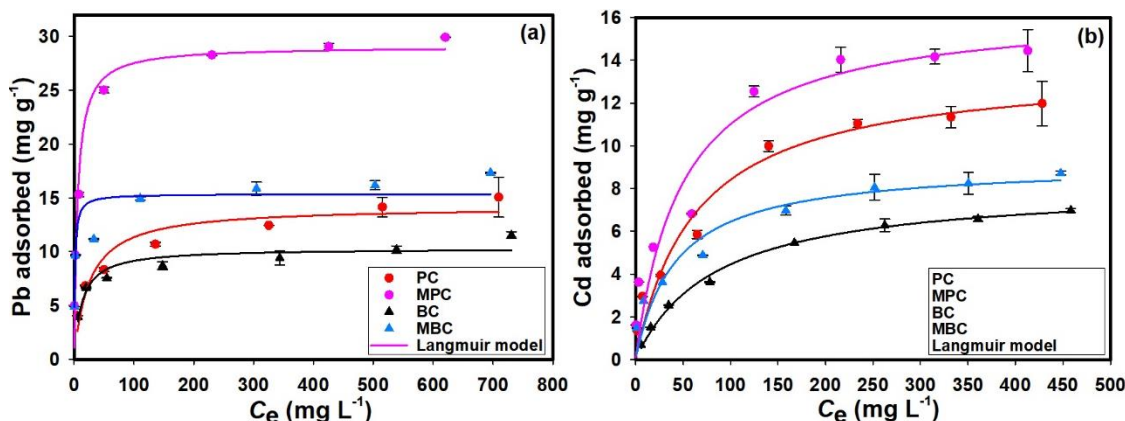


Fig. 6. Sorption isotherms of pristine and modified biochars: (a) Pb (II), (b) Cd (II)

Table 3. Isotherm Parameters of Pb (II) and Cd (II) Adsorption onto Biochar

Heavy metal	Biochar	Langmuir			Freundlich			Temkin		
		q_{max} (mg g ⁻¹)	K_L (L mg ⁻¹)	R^2	1/n	K_F (mg ⁽¹⁻ⁿ⁾ L ⁿ g ⁻¹)	R^2	b	K_T (L g ⁻¹)	R^2
Pb (II)	PC	15.40	0.025	0.991	0.256	2.911	0.974	1.016	2.223	0.992
	MPC	29.95	0.140	0.999	0.225	8.218	0.943	15.281	3.373	0.977
	BC	11.37	0.032	0.987	0.194	3.196	0.903	3.637	1.393	0.963
	MBC	17.15	0.083	0.997	0.152	6.678	0.860	76.090	1.574	0.946
Cd (II)	PC	12.98	0.023	0.983	0.406	9.612	0.977	0.550	2.120	0.930
	MPC	15.38	0.035	0.979	0.320	9.519	0.974	2.435	2.000	0.878
	BC	8.04	0.013	0.996	0.523	9.918	0.966	0.189	1.541	0.981
	MBC	9.14	0.029	0.987	0.307	9.709	0.983	1.281	1.299	0.932

CONCLUSIONS

1. The UV-irradiated biochar exhibited greater hydrophilicity, lower pH, larger surface area, increased porosity and abundant oxygen-containing functional groups in comparison to the original biochar.
2. The modification was mainly attributable to the photooxidation mechanism. The photochemical reactions were responsible for the dissociation of the carbon-carbon bond and the formation of the carbon-oxygen bond on the biochar surface, resulting in the development of the pore structure and the formation of oxygenic groups.
3. The UV-modified biochar showed a significant increase in the adsorption capacity of metal ions in water. The kinetics and isotherms of biochar sorption could be well described by the pseudo-second-order model and the Langmuir model, except that the Cd(II) adsorption could be better predicted by the Elovich model.
4. The UV-modified biochar had comparable adsorption performances to many other biochar produced from ligneous plant biomass. The effects of UV irradiation at different wavelengths on the surface properties of biochar deserve further investigation.

ACKNOWLEDGEMENTS

The authors gratefully acknowledge financial support from Research Project of Power China (No. P42819, No. P45220) and Large Instruments and Equipment Open Fund of Chongqing University (grant number: 202303150125).

REFERENCES

- Asmatulu, R., Mahmud, G. A., Hille, C., and Misak, H. E. (2011). "Effects of UV degradation on surface hydrophobicity, crack, and thickness of MWCNT-based nanocomposite coatings," *Prog. Org. Coat.* 72(3), 553-561. DOI: 10.1016/j.porgcoat.2011.06.015
- Asuquo, E., Martin, A., Nzerem, P., Siperstein, F., and Fan, X. L. (2017). "Adsorption of Cd (II) and Pb (II) ions from aqueous solutions using mesoporous activated carbon adsorbent: Equilibrium, kinetics and characterisation studies," *J. Environ. Chem. Eng.* 5(1), 679-698. DOI: 10.1016/j.jece.2016.12.043
- Beamson, G., and Briggs, D. R. (1992). "15 The Database," in: *High Resolution XPS of Organic Polymers: The Scienta ESCA300 Database*, John Wiley & Sons, Chichester, UK.
- Brunauer, S., Deming, L. S., Deming, W. E., and Teller, E. (1940). "On a theory of the van der Waals adsorption of gases," *J. Am. Chem. Soc.* 62, 1723-1732. DOI: 10.1021/ja01864a025
- Carter, M. R., and Gregorich, E. G. (2006). "Ion exchange and exchangeable cations," in: *Soil Sampling and Methods of Analysis*, 2nd Edition, Taylor & Francis Group Boca Raton, FL, USA.
- Chen, B. L., Zhou, D. D., and Zhu, L. Z. (2008). "Transitional adsorption and partition of nonpolar and polar aromatic contaminants by biochars of pine needles with different

- pyrolytic temperatures,” *Environ. Sci. Technol.* 42(14), 5137-5143. DOI: 10.1021/es8002684
- Cheng, Y. C., Kaloni, T. P., Zhu, Z. Y., and Schwingenschlögl, U. (2012). “Oxidation of graphene in ozone under ultraviolet light,” *Appl. Phys. Lett.* 101(7), 073110. DOI: 10.1063/1.4746261
- Chu, B., Amano, Y., and Machida, M. (2019). “Preparation of bamboo-based oxidized biochar for simultaneous removal of Cd(II) and Cr(VI) from aqueous solutions,” *Desalin. Water Treat.* 168, 269-281. DOI: 10.5004/dwt.2019.24653
- Ghasemi-Kahrizsangi, A., Neshati, J., Shariatpanahi, H., and Akbarinezhad, E. (2015). “Improving the UV degradation resistance of epoxy coatings using modified carbon black nanoparticles,” *Prog. Org. Coat.* 85, 199-207. DOI: 10.1016/j.porgcoat.2015.04.011
- Hou, J. F., Yu, J. L., Li, W. X., He, X. D., and Li, X. D. (2022). “The effects of chemical oxidation and high-temperature reduction on surface functional groups and the adsorption performance of biochar for sulfamethoxazole adsorption,” *Agronomy-Basel* 12(2), article 510. DOI: 10.3390/agronomy12020510
- Hubbe, M. A., Azizian, S., and Douven, S. (2019). “Implications of apparent pseudo-second-order adsorption kinetics onto cellulosic materials. A review,” *BioResources* 14(3), 7582-7626. DOI: 10.15376/biores.14.3.7582-7626
- Jin, H. M., Capareda, S., Chang, Z. Z., Gao, J., Xu, Y. D., and Zhang, J. Y. (2014). “Biochar pyrolytically produced from municipal solid wastes for aqueous As(V) removal: Adsorption property and its improvement with KOH activation,” *Bioresource Technol.* 169, 622-629. DOI: 10.1016/j.biortech.2014.06.103
- Karthik, V., Karuna, B., Jeyanthi, J., and Periyasamy, S. (2023). “Biochar production from seeds, activation and characterization for effective removal of Cu ions in polluted drinking water,” *Biomass Convers. Bior.* 13(11), 9381-9395. DOI: 10.1007/s13399-022-03627-2
- Kryszak, M., Parekh, B., Debies, T., Dileo, R. A., Landi, B. J., Raffaele, R. P., and Takacs, G. A. (2007). “Gas-phase surface functionalization of multi-walled carbon nanotubes with vacuum UV photo-oxidation,” *J. Adhes. Sci. Technol.* 21(10), 999-1007. DOI: 10.1163/156856107781393893
- Kumar, A., Bhattacharya, T., Shaikh, W. A., Chakraborty, S., Sarkar, D., and Biswas, J. K. (2022). “Biochar modification methods for augmenting sorption of contaminants,” *Curr. Pollut. Rep.* 8(4), 519-555. DOI: 10.1007/s40726-022-00238-3
- Kwan, Y. C. G., Ng, G. M., and Huan, C. H. A. (2015). “Identification of functional groups and determination of carboxyl formation temperature in graphene oxide using the XPS O 1s spectrum,” *Thin Solid Films* 590, 40-48. DOI: 10.1016/j.tsf.2015.07.051
- Li, H. B., Dong, X. L., da Silva, E. B., de Oliveira, L. M., Chen, Y. S., and Ma, L. N. Q. (2017). “Mechanisms of metal sorption by biochars: Biochar characteristics and modifications,” *Chemosphere* 178, 466-478. DOI: 10.1016/j.chemosphere.2017.03.072
- Li, J. L., Kudin, K. N., McAllister, M. J., Prud'homme, R. K., Aksay, I. A., and Car, R. (2006). “Oxygen-driven unzipping of graphitic materials,” *Phys. Rev. Lett.* 96(17), article 176101. DOI: 10.1103/PhysRevLett.96.176101
- Li, Q., Ding, W. C., Yong, Y., Zeng, X. L., and Gao, Y. T. (2016). “Effects of ultraviolet modification on physicochemical property and adsorption performance of biochar,” *Nanosci. Nanotech. Lett.* 8(11), 978-984. DOI: 10.1166/nnl.2016.2184

- Liu, Z. G., and Zhang, F. S. (2009). "Removal of lead from water using biochars prepared from hydrothermal liquefaction of biomass," *J.Hazard. Mater.* 167(1-3), 933-9. DOI: 10.1016/j.jhazmat.2009.01.085
- Liu, X., Xu, X., Dong, X., and Park, J. (2019). "Adsorption characteristics of cadmium ions from aqueous solution onto pine sawdust biomass and biochar," *BioResources* 14(2), 4270-4283. DOI: 10.15376/biores.14.2.4270-4283
- Manfrin, J., Gonçalves, A. J. r., Schwantes, D., Zimmermann, J., and Conradi, E. J. r. (2021). "Effective Cd removal from water using novel micro-mesoporous activated carbons obtained from tobacco: CCD approach, optimization, kinetic, and isotherm studies," *J. Environ. Health Sci.* 19(2), 1851-1874. DOI:10.1007/s40201-021-00740-8
- Mohan, D., Kumar, H., Sarswat, A., Alexandre-Franco, M., and Pittman, C. U. (2014). "Cadmium and lead remediation using magnetic oak wood and oak bark fast pyrolysis bio-chars," *Chem. Eng. J.* 236, 513-528. DOI: 10.1016/j.cej.2013.09.057
- Mohan, D., Kumar, H., Sarswat, A., Alexandre-Franco, M., and Pittman, C. U. (2014). "Cadmium and lead remediation using magnetic oak wood and oak bark fast pyrolysis bio-chars," *Chem. Eng. J.* 236, 513-28. DOI: 10.1016/j.cej.2013.09.057
- Mohan, D., Pittman, C. U., Bricka, M., Smith, F., Yancey, B., Mohammad, J., Steele, P. H., Alexandre-Franco, M. F., Gómez-Serrano, V., and Gong, H. (2007). "Sorption of arsenic, cadmium, and lead by chars produced from fast pyrolysis of wood and bark during bio-oil production," *J. Colloid Interf. Sci.* 310(1), 57-73. DOI: 10.1016/j.jcis.2007.01.020
- Nightingale, E. R. (1959). "Phenomenological theory of ion solvation – Effective radii of hydrated ions," *J. Phy. Chem.* 63(9), 1381-1387. DOI: 10.1021/j150579a011
- Osbeck, S., Bradley, R. H., Liu, C., Idriss, H., and Ward, S. (2011). "Effect of an ultraviolet/ozone treatment on the surface texture and functional groups on polyacrylonitrile carbon fibres," *Carbon* 49(13), 4322-4330. DOI: 10.1016/j.carbon.2011.06.005
- Parekh, B., Debies, T., Knight, P., Santhanam, K. S. V., and Takacs, G. A. (2006). "Surface functionalization of multiwalled carbon nanotubes with UV and vacuum UV photo-oxidation," *J. Adhes. Sci. Technol.* 20(16), 1833-1846. DOI: 10.1163/156856106779116641
- Peng, Z. Y., Zhao, H., Lyu, H. H., Wang, L., Huang, H., Nan, Q., and Tang, J. C. (2018). "UV modification of biochar for enhanced hexavalent chromium removal from aqueous solution," *Environ. Sci. Poll. Res.* 25(11), 10808-10819. DOI: 10.1007/s11356-018-1353-3
- Raja, M. (2015). "Surface modification of carbon nanotubes with combined UV and ozone treatments," *Fuller. Nanotub. Car. N.* 23(1), 11-16. DOI: 10.1080/1536383X.2014.885960
- Singh, E., Kumar, A., Mishra, R., You, S. M., Singh, L., Kumar, S., and Kumar, R. (2021). "Pyrolysis of waste biomass and plastics for production of biochar and its use for removal of heavy metals from aqueous solution," *Bioresource Technol.* 320, article 124278. DOI: 10.1016/j.biortech.2020.124278
- Tan, K. T., White, C. C., Benatti, D. J., and Hunston, D. L. (2010). "Effects of ultraviolet radiation, temperature and moisture on aging of coatings and sealants – A chemical and rheological study," *Polym. Degrad. Stabil.* 95(9), 1551-1556. DOI: 10.1016/j.poly.mdegradstab.2010.06.008
- Trakal, L., Bingöl, D., Pohorely, M., Hruska, M., and Komárek, M. (2014). "Geochemical and spectroscopic investigations of Cd and Pb sorption mechanisms on

- contrasting biochars: Engineering implications,” *Bioresource Technol.* 171, 442-451. DOI: 10.1016/j.biortech.2014.08.108
- Wang, J. J., and Liu, F. (2013). “Enhanced adsorption of heavy metal ions onto simultaneous interpenetrating polymer network hydrogels synthesized by UV irradiation,” *Polym. Bull.* 70(4), 1415-1430. DOI: 10.1007/s00289-013-0934-z
- Wang, M. C., Sheng, G. D., and Qiu, Y. P. (2015). “A novel manganese-oxide/biochar composite for efficient removal of lead(II) from aqueous solutions,” *Int. J. Environ. Sci. Te.* 12(5), 1719-1726. DOI: 10.1007/s13762-014-0538-7
- Wang, Y., Wang, X. J., Wang, X., Liu, M. A., Yang, L. Z., Wu, Z., Xia, S. Q., and Zhao, J. F. (2012). “Adsorption of Pb(II) in aqueous solutions by bamboo charcoal modified with KMnO via microwave irradiation,” *Colloid. Surface. A.* 414, 1-8. DOI: 10.1016/j.colsurfa.2012.08.007
- Wang, Z. Y., Liu, G. C., Zheng, H., Li, F. M., Ngo, H. H., Guo, W. S., Liu, C., Chen, L., and Xing, B. S. (2015). “Investigating the mechanisms of biochar’s removal of lead from solution,” *Bioresource Technol.* 177, 308-317. DOI: 10.1016/j.biortech.2014.11.077
- Wu, F. C., Tseng, R. L., and Juang, R. S. (2009). “Characteristics of Elovich equation used for the analysis of adsorption kinetics in dye-chitosan systems,” *Chem. Eng. J.* 150(2-3), 366-373. DOI: 10.1016/j.cej.2009.01.014
- Xiao, Y. L., Xue, Y. W., Gao, F., and Mosa, A. (2017). “Sorption of heavy metal ions onto crayfish shell biochar: Effect of pyrolysis temperature, pH and ionic strength,” *J. Taiwan Inst. Chem. E.* 80, 114-121. DOI: 10.1016/j.jtice.2017.08.035
- Yin, Q. Q., Wang, R. K., and Zhao, Z. H. (2018). “Application of Mg-Al-modified biochar for simultaneous removal of ammonium, nitrate, and phosphate from eutrophic water,” *J. Clean. Prod.* 176, 230-240. DOI: 10.1016/j.jclepro.2017.12.117
- Zeng, Y., Lin, Y. H., Ma, M., and Chen, H. (2024). “A review on the removal of heavy metals from water by phosphorus-enriched biochar,” *Minerals* 14(1), article 61. DOI: 10.3390/min14010061
- Zhang, X., Zhang, S. H., Yang, H. P., Feng, Y., Chen, Y. Q., Wang, X. H., and Chen, H. P. (2014). “Nitrogen enriched biochar modified by high temperature CO-ammonia treatment: Characterization and adsorption of CO,” *Chem. Eng. J.* 257, 20-27. DOI: 10.1016/j.cej.2014.07.024
- Zhao, X. X., Tuo, B. Y., Long, S., Song, X., Wan, L., and Xiang, H. C. (2021). “Study on adsorption of Cd by Ti-pillared montmorillonite-mixed activated carbon,” *Micro Nano Lett.* 16(5), 304-312. DOI: 10.1049/mna2.12052
- Zhou, Y. M., Gao, B., Zimmerman, A. R., Fang, J., Sun, Y. N., and Cao, X. D. (2013). “Sorption of heavy metals on chitosan-modified biochars and its biological effects,” *Chem. Eng. J.* 231, 512-518. DOI: 10.1016/j.cej.2013.07.036

Article submitted: June 3, 2024; Peer review completed: July 11, 2024; Revised version received: August 5, 2024; Accepted: August 10, 2024; Published: August 27, 2024.
DOI: 10.15376/biores.19.4.7566-7590

APPENDIX

Supplementary Information

Table S1. Dynamics Parameters for Pb (II) and Cd (II) Adsorption on Biochar

Metal		Pb				Cd			
Biochar		PC	MPC	BC	MBC	PC	MPC	BC	MBC
$q_{e,exp}$ (mg g^{-1})		10.56	24.69	8.49	14.71	5.81	6.63	3.49	4.38
First-order model	$q_{e,cal}$ (mg g^{-1})	4.98	20.39	6.27	5.87	1.56	1.61	0.67	0.66
	k_1 (h^{-1})	0.004	0.003	0.005	0.003	0.134	0.158	0.164	0.121
	R^2	0.854	0.985	0.895	0.831	0.791	0.790	0.971	0.867
	NSD(%)	70.40	34.47	61.00	78.44	95.17	95.60	97.88	100.84
Second-order model	$q_{e,cal}$ (mg g^{-1})	10.93	26.18	8.80	15.04	5.84	6.67	3.51	4.39
	k_2 ($\text{gmg}^{-1}\text{h}^{-1}$)	0.073	0.018	0.085	0.073	0.421	0.461	1.158	1.072
	R^2	0.999	0.998	0.999	0.999	0.999	1.000	1.000	1.000
	NSD(%)	28.69	18.10	13.81	25.78	13.83	11.28	16.72	14.69
Elovich model	α (mg g^{-1})	4.91	9.55	3.87	7.67	4.06	4.73	2.92	3.72
	β ($\text{mg g}^{-1}\text{h}^{-1}$)	1.932	4.800	1.514	2.433	0.576	0.653	0.176	0.208
	R^2	0.890	0.958	0.940	0.860	0.880	0.860	0.964	0.940
	NSD(%)	39.46	20.17	16.65	49.97	8.69	9.23	1.95	2.53

Table S2. Comparison of Pb (II) Adsorption Capacities of Various Biochar

Biochar	pH	Temp. (°C)	Reaction time (h ⁻¹)	Surface area (m ² g ⁻¹)	Adsorption capacity (mg g ⁻¹)	Reference
Magnetic oak wood char	5.0	25	48	6.1	10.13	(Mohan <i>et al.</i> 2014)
Bamboo charcoal	5.0	25	48	15.5	25.03	(Wang <i>et al.</i> 2012)
KMnO ₄ modified bamboo charcoal	5.0	25	48	172.3	55.56	
Pine wood char	5.0	25	24	2.73	4.13	(Mohan <i>et al.</i> 2007)
Oak wood char	5.0	25	24	2.04	2.62	
Pinewood biochar	5.0	25	24	--	3.89	(Liu & Zhang 2009)
Pine wood biochar	5.0	25	48	369	18.13	(Wang <i>et al.</i> 2015)
HMO-loaded Pine wood biochar	5.0	25	48	194	91.98	
Chitosan modified bamboo biochar	4.5	22	32	169	14.3	(Zhou <i>et al.</i> 2013)
Pinewood biochar	5.0	25	24	280.86	15.40	This work
UV irradiated pinewood biochar	5.0	25	24	457.72	29.95	This work
Bamboo biochar	5.0	25	24	141.73	11.37	This work
UV irradiated bamboo biochar	5.0	25	24	449.13	17.15	This work

Table S3. Comparison of Cd (II) Adsorption Capacities of Various Biochar

Biochar	pH	Temp. (°C)	Reaction time (h ⁻¹)	Surface area (m ² g ⁻¹)	Adsorption capacity (mg g ⁻¹)	Reference
Pine sawdust biochar	6.5	25	5	321	6.09	(Liu <i>et al.</i> 2019)
Oxidized bamboo biochar	6.0	25	3	1120	30.3	(Chu <i>et al.</i> 2019)
Magnetic oak wood char	5.0	25	48	6.1	2.87	(Mohan <i>et al.</i> 2014)
Magnetic oak bark char	5.0	25	48	8.8	7.40	
Oak wood char	5.0	25	24	2.04	0.37	(Mohan <i>et al.</i> 2007)
Oak bark char	5.0	25	24	25.4	5.40	
Pine bark char	5.0	25	24	1.88	0.34	
Pinewood biochar	5.0	25	24	280.86	12.98	This work
UV irradiated pinewood biochar	5.0	25	24	457.72	15.38	This work
Bamboo biochar	5.0	25	24	141.73	8.04	This work
UV irradiated bamboo biochar	5.0	25	24	449.13	9.14	This work

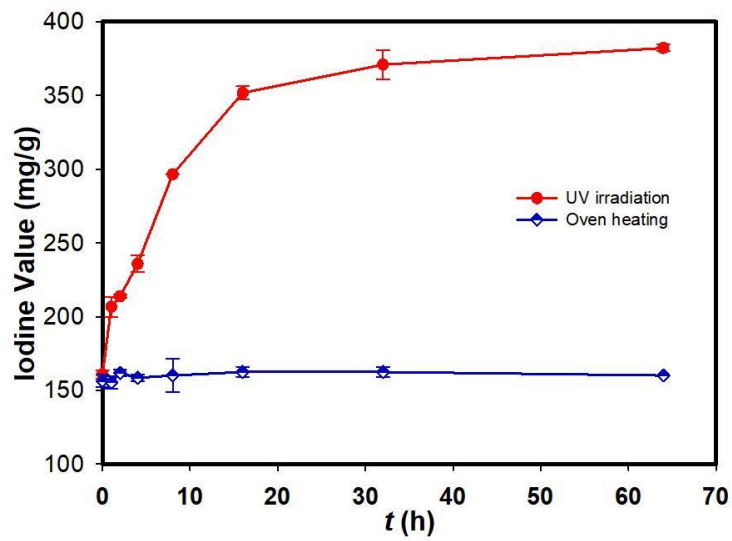


Fig. S1. Iodine value of biochar versus UV irradiation time (Initial iodine concentration: 0.1 mol/L, oven temperature: 100 °C, adsorption time: 15 min)

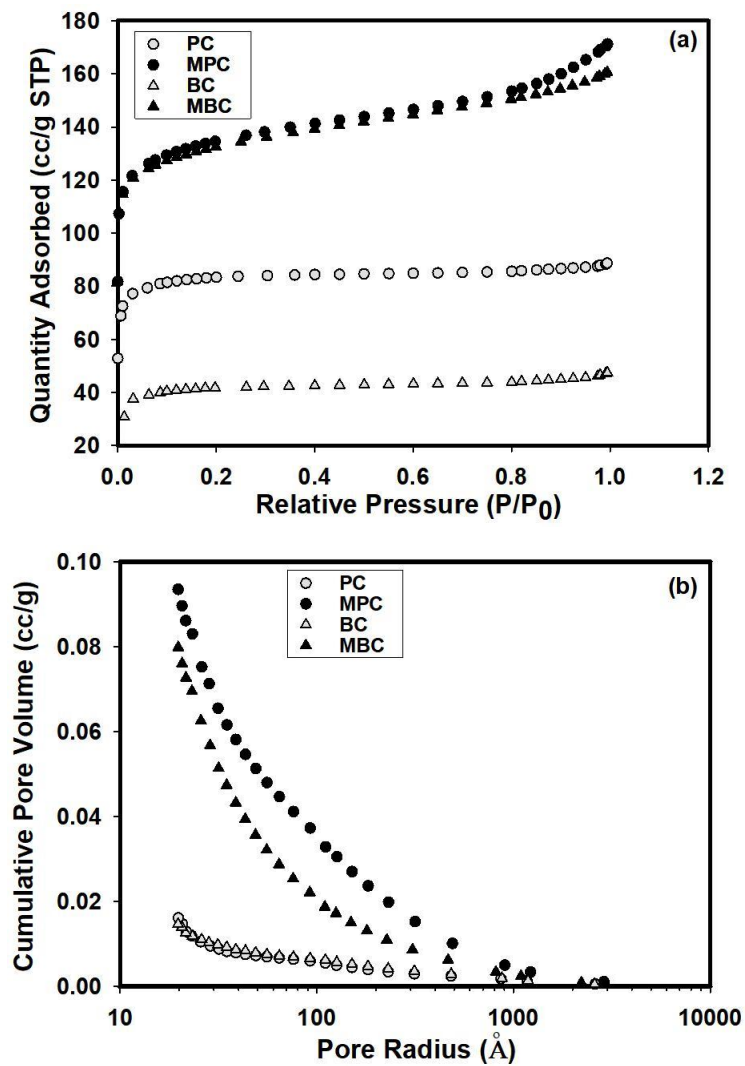


Fig. S2. Adsorption isotherms (a) for N_2 at 77K and pore size distribution (b) of biochars (outgas temperature: 300°C, outgas time: 10.0 h)

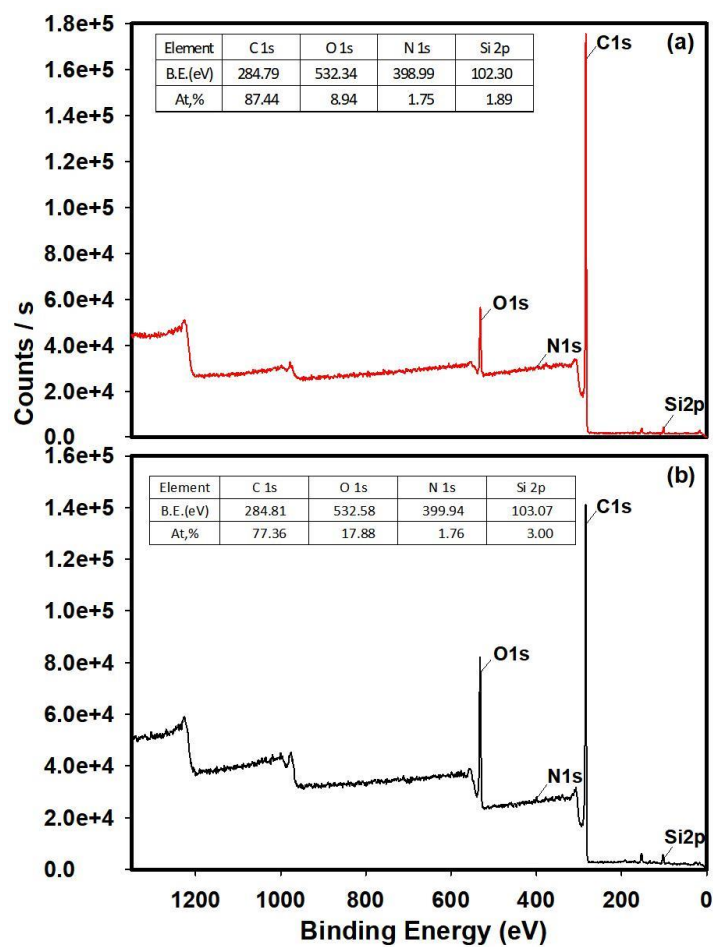


Fig. S3. XPS full survey scan of PC and MPC: (a) PC; (b) MPC (C 1s = 284.80eV)

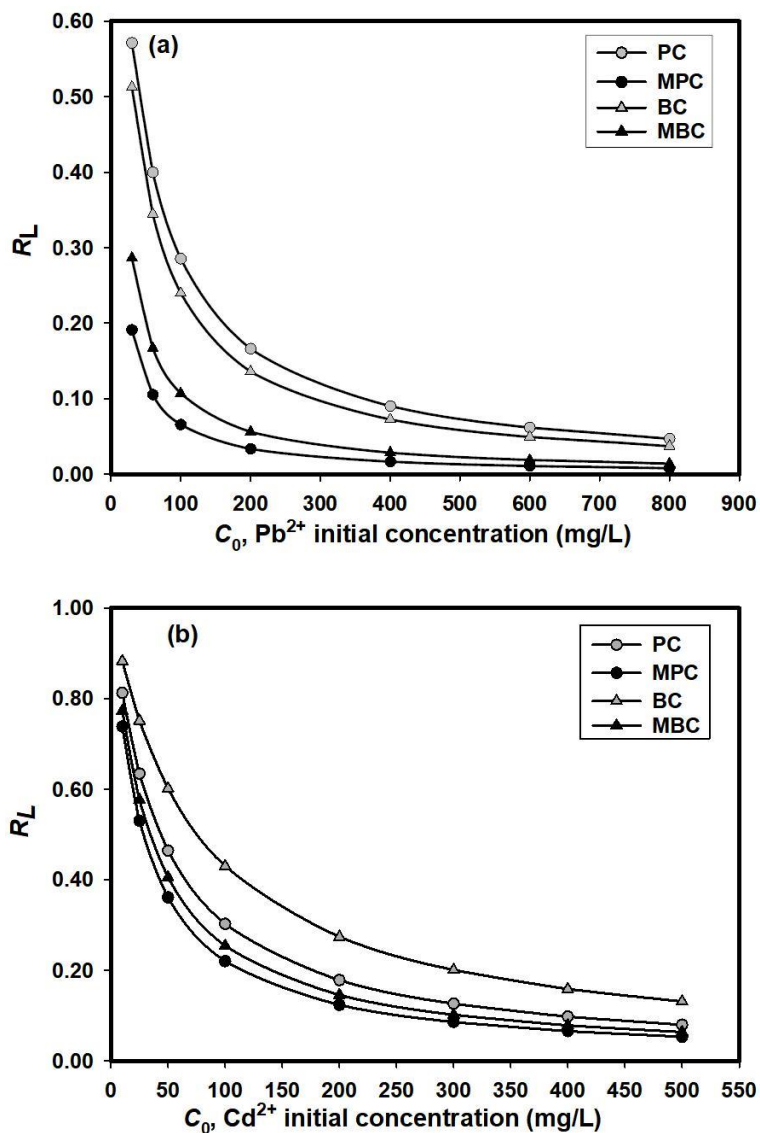


Fig. S4. Separation parameter R_L of adsorption isotherms: (a) Pb^{2+} , (b) Cd^{2+} (sorbent dosage: 6g L^{-1} , temperature: $25 \pm 1.0^\circ C$, initial pH: 5.0, equilibrium: 24 h)